A Dual-Catalysis Approach to Enantioselective [2 + 2] Photocycloadditions Using Visible Light

Juana Du *et al.*

Science **344**, 392 (2014);
DOI: 10.1126/science.1251511

individual neurons from each line can readily be identified. Whereas some lines drive expression in a single pair of neurons, most drive in the range of two to five candidate neuron types. In cases where lines drive in more than one neuron, intersectional strategies can be used to target individual neurons and test the effect of their activation on behavior (*2*).

This reference atlas provides a valuable starting point for understanding how distinct behaviors are selected and controlled. Large-scale connectomics (*31*–*33*) and functional brain imaging methods (*34*, *35*) will soon provide similarly comprehensive views of the structure of neural circuits and of the activity patterns within those circuits. However, a connectome by itself does not carry information about which neurons mediate which behaviors. Similarly, a brain-activity map alone shows the flow of information through the network, but does not reveal causal relationships between neurons and behavior. Together, the neuron-behavior map, the neuron-activity map, and the connectome complement one another, laying the groundwork for a brainwide understanding of the principles by which brains generate behavior.

The statistical methods presented here are generally applicable to discovery of scientifically meaningful structure from big data—a pressing problem in the information age.

References and Notes

1. B. D. Pfeiffer *et al.*, *Proc. Natl. Acad. Sci. U.S.A.* **105**, 9715–9720 (2008).
2. B. D. Pfeiffer *et al.*, *Genetics* **186**, 735–755 (2010).
3. A. Jenett *et al.*, *Cell Rep.* **2**, 991–1001 (2012).
4. N. A. Swierczek, A. C. Giles, C. H. Rankin, R. A. Kerr, *Nat. Methods* **8**, 592–598 (2011).
5. K. Branson, A. A. Robie, J. Bender, P. Perona, M. H. Dickinson, *Nat. Methods* **6**, 451–457 (2009).
6. M. Kabra, A. A. Robie, M. Rivera-Alba, S. Branson, K. Branson, *Nat. Methods* **10**, 64–67 (2013).
7. C. Schroll *et al.*, *Curr. Biol.* **16**, 1741–1747 (2006).
8. R. Y. Hwang *et al.*, *Curr. Biol.* **17**, 2105–2116 (2007).
9. C. W.-H. Wu *et al.*, *Neuron* **70**, 229–243 (2011).
10. T. Ohyama *et al.*, *PLOS ONE* **8**, e71706 (2013).
11. C. E. Priebe, D. J. Marchette, D. M. Healy, *Mod. Signal Process.* **46**, 223 (2003).
12. W. K. Allard, G. Chen, M. Maggioni, *Appl. Comput. Harmon. Anal.* **32**, 435–462 (2012).
13. P. Bendich, D. Cohen-Steiner, H. Edelsbrunner, J. Harer, D. Morozov, in *48th Annual IEEE Symposium on Foundations of Computer Science (FOCS'07)* (IEEE, Providence, RI, 2007), pp. 536–546.
14. K. E. Giles, M. W. Trosset, D. J. Marchette, C. E. Priebe, *Comput. Stat.* **23**, 497–517 (2008).
15. C. E. Priebe, D. J. Marchette, D. M. Healy, *IEEE Trans. Pattern Anal. Mach. Intell.* **26**, 699–708 (2004).
16. D. Karakos, S. Khudanpur, J. Eisner, C. E. Priebe, in *Proceedings of the 2005 IEEE International Conference on Acoustics Speech and Signal Processing ICASSP* (IEEE, Philadelphia, 2005), vol. 5, pp. 1081–1084.
17. C. E. Priebe, *IEEE Trans. Pattern Anal. Mach. Intell.* **23**, 404–413 (2001).
18. I. Borg, P. J. F. Groenen, *Modern Multidimensional Scaling: Theory and Applications* (Springer, New York, 2010).
19. T. Hastie, R. Tibshirani, J. Friedman, *The Elements of Statistical Learning: Data Mining, Inference, and Prediction* (Springer, New York, 2001).
20. E. A. Kane *et al.*, *Proc. Natl. Acad. Sci. U.S.A.* **110**, E3868–E3877 (2013).
21. M. Kernan, D. Cowan, C. Zuker, *Neuron* **12**, 1195–1206 (1994).
22. J. A. Ainsley *et al.*, *Curr. Biol.* **13**, 1557–1563 (2003).
23. M. Tang, Y. Park, C. E. Priebe, http://arxiv.org/abs/1305.4893 (2013).
24. P. I. Good, *Permutation, Parametric, and Bootstrap Tests of Hypotheses* (Springer, New York, 2010).
25. D. Yekutieli, Y. Benjamini, *Ann. Stat.* **29**, 1165–1188 (2001).
26. R. A. Fisher, *Statistical Methods for Research Workers* (Oliver and Boyd, Edinburgh, 1925).
27. G. Struhl, K. Basler, *Cell* **72**, 527–540 (1993).
28. I. Kupfermann, K. R. Weiss, *Behav. Brain Sci.* **1**, 3–10 (1978).
29. B. Hedwig, *J. Neurophysiol.* **83**, 712–722 (2000).
30. A. E. X. Brown, E. I. Yemini, L. J. Grundy, T. Jucikas, W. R. Schafer, *Proc. Natl. Acad. Sci. U.S.A.* **110**, 791–796 (2013).
31. D. D. Bock *et al.*, *Nature* **471**, 177–182 (2011).
32. M. Helmstaedter, *Nat. Methods* **10**, 501–507 (2013).
33. S.-Y. Takemura *et al.*, *Nature* **500**, 175–181 (2013).
34. M. B. Ahrens, M. B. Orger, D. N. Robson, J. M. Li, P. J. Keller, *Nat. Methods* **10**, 413–420 (2013).
35. T. Schrödel, R. Prevedel, K. Aumayr, M. Zimmer, A. Vaziri, *Nat. Methods* **10**, 1013–1020 (2013).

Acknowledgments: We thank G. M. Rubin, B. D. Pfeiffer, A. Nern, and B. Condron for fly stocks; B. D. Mensh for exceptionally helpful comments on the manuscript; A. Cardona, J. H. Simpson, and K. Branson for helpful discussions; C. Sullivan and A. Mondal for help with editing; H. Li and Fly Light Project Team at Janelia HHMI for images of neuronal lines; Janelia Fly Core for setting up the fly crosses for the activation screen; and Janelia Scientific Computing for help with data processing and storage, especially E. Trautman, R. Svirskas, and D. Olbris. Supported by the Larval Olympiad Project and Janelia HHMI, the XDATA program of the Defense Advanced Research Projects Agency administered through Air Force Research Laboratory contract FA8750-12-2-0303, and a National Security Science and Engineering Faculty Fellowship. All raw data, data derivatives, and code are freely available from http://openconnecto.me/behaviotypes.

Supplementary Materials

www.sciencemag.org/content/344/6182/386/suppl/DC1
Materials and Methods
Figs. S1 to S6
Movies S1 to S58
Supplementary Data Sets 1 and 2
References (*36*–*40*)

31 December 2013; accepted 17 March 2014
Published online 27 March 2014;
10.1126/science.1250298

REPORTS

A Dual-Catalysis Approach to Enantioselective [2 + 2] Photocycloadditions Using Visible Light

Juana Du,* Kazimer L. Skubi,* Danielle M. Schultz,* Tehshik P. Yoon†

In contrast to the wealth of catalytic systems that are available to control the stereochemistry of thermally promoted cycloadditions, few similarly effective methods exist for the stereocontrol of photochemical cycloadditions. A major unsolved challenge in the design of enantioselective catalytic photocycloaddition reactions has been the difficulty of controlling racemic background reactions that occur by direct photoexcitation of substrates while unbound to catalyst. Here, we describe a strategy for eliminating the racemic background reaction in asymmetric [2 + 2] photocycloadditions of α,β-unsaturated ketones to the corresponding cyclobutanes by using a dual-catalyst system consisting of a visible light–absorbing transition-metal photocatalyst and a stereocontrolling Lewis acid cocatalyst. The independence of these two catalysts enables broader scope, greater stereochemical flexibility, and better efficiency than previously reported methods for enantioselective photochemical cycloadditions.

Modern stereoselective synthesis enables the construction of a vast array of organic molecules with precise control over their three-dimensional structure (*1*, *2*), which is important in a variety of fields ranging from drug discovery to materials engineering. Photochemical reactions could have a substantial impact on these fields by affording direct access to certain structural motifs that are otherwise difficult to construct (*3*, *4*). For example, the most straightforward methods for the construction of cyclobutanes and other strained four-membered rings are photochemical [2 + 2] cycloaddition reactions. The stereochemical control of photocycloadditions, however, remains much more challenging than the stereocontrol of analogous non-photochemical reactions (*5*, *6*) despite the chemistry community's sustained interest in photochemical stereoinduction over the last century (*7*, *8*).

Although many strategies using covalent chiral auxiliaries (*9*, *10*) or noncovalent chiral controllers (*11*, *12*) have been used to dictate absolute stereochemistry in photochemical cycloaddition reactions, the development of methods that utilize substoichiometric stereodifferentiating chiral catalysts has proven a more formidable challenge.

Department of Chemistry, University of Wisconsin–Madison, 1101 University Avenue, Madison, WI 53706, USA.

*These authors contributed equally to this work.
†Corresponding author. E-mail: tyoon@chem.wisc.edu

This is largely due to the difficulty of controlling uncatalyzed background photochemical processes (Fig. 1A, path i). The direct photoexcitation of an unbound achiral substrate, free from the influence of a chiral catalyst, necessarily results in racemic products; thus, regardless of how enantioselective the catalyzed reaction might be (Fig. 1A, path ii), the net enantiomeric excess (ee) of the product will be low unless the rate of the uncatalyzed

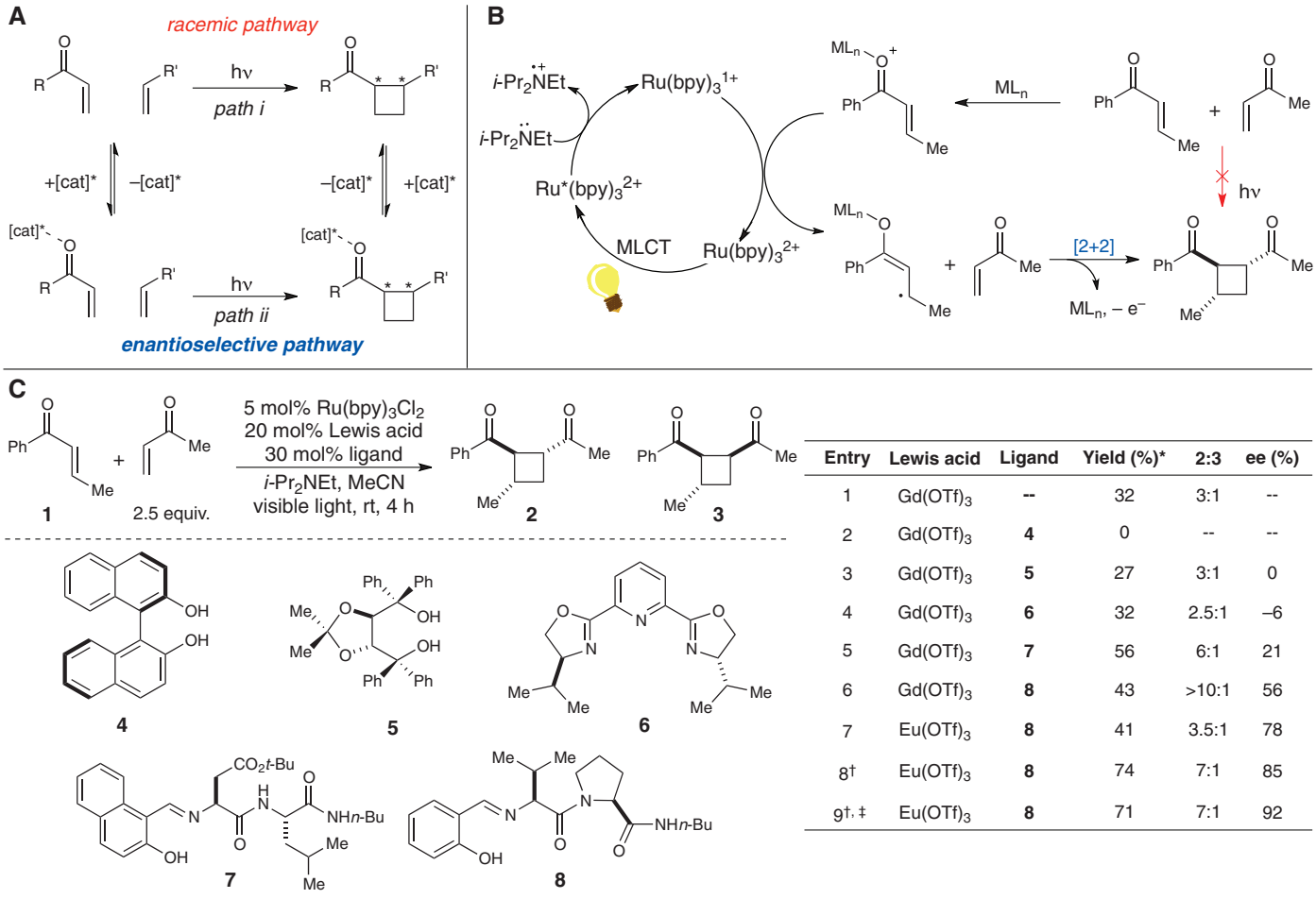

Entry	Lewis acid	Ligand	Yield (%)*	2:3	ee (%)
1	$Gd(OTf)_3$	--	32	3:1	--
2	$Gd(OTf)_3$	**4**	0	--	--
3	$Gd(OTf)_3$	**5**	27	3:1	0
4	$Gd(OTf)_3$	**6**	32	2.5:1	–6
5	$Gd(OTf)_3$	**7**	56	6:1	21
6	$Gd(OTf)_3$	**8**	43	>10:1	56
7	$Eu(OTf)_3$	**8**	41	3.5:1	78
8†	$Eu(OTf)_3$	**8**	74	7:1	85
9†,‡	$Eu(OTf)_3$	**8**	71	7:1	92

Fig. 1. Design plan for enantioselective catalytic [2 + 2] cycloaddition reactions. (**A**) Competing enantioselective and racemic pathways in asymmetric photocycloadditions. (**B**) $Ru(bpy)_3^{2+}$-catalyzed [2 + 2] cycloaddition reaction using visible light. bpy, 2,2′-bipyridine; MLCT, metal-to-ligand charge transfer. (**C**) Survey of chiral Lewis acid cocatalysts. OTf, trifluoromethanesulfonate. rt, room temperature. *Yields determined by ^{1}H–nuclear magnetic resonance (NMR) analysis using an internal standard. †Optimized conditions: 5 equivalents of methyl vinyl ketone, 5 mol % Ru $(bpy)_3Cl_2$, 10 mol % Lewis acid, 20 mol % ligand, 0.2 M MeCN, 2 hours. ‡Reaction conducted at –20°C for 15 hours.

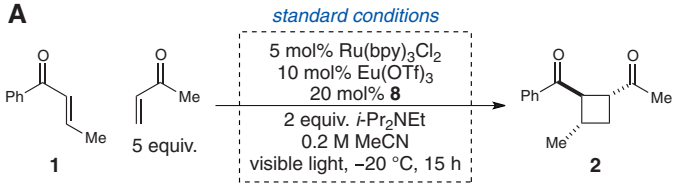

Entry	Variation from standard conditions	Yield (%)
1	none	71
2	no light	0
3	no $Ru(bpy)_3Cl_2$	0
4	no $Eu(OTf)_3$	0
5	no *i*-Pr_2NEt	0

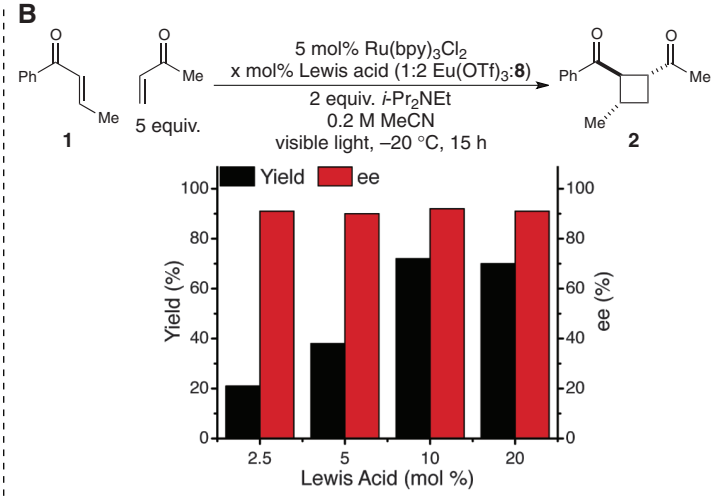

Fig. 2. Control experiments for the asymmetric visible light–photocatalyzed [2 + 2] cycloaddition. (**A**) Omission of any reaction component results in no [2 + 2] cycloaddition. (**B**) Enantioselectivity of the photocatalyzed [2 + 2] cycloaddition is not affected by the concentration of chiral Lewis acid catalyst.

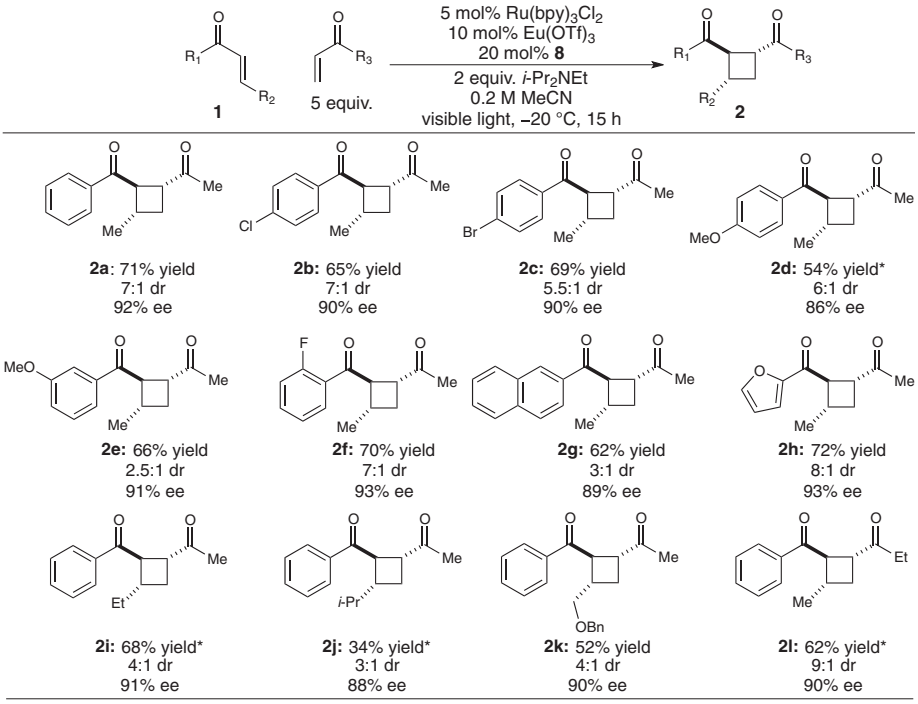

Fig. 3. Substrate scope of the enantioselective [2 + 2] cycloaddition reaction. Diastereomer ratios (dr) measured by ^{1}H-NMR analysis of the unpurified reaction mixtures. Reported yields represent total isolated yields of the 1,2-*cis* and 1,2-*trans* isomers. For each entry, yields represent the average of two reproducible experiments. *Reaction conducted for 24 hours.

racemic background cycloaddition can be diminished. Bach, whose laboratory has reported the only highly enantioselective catalytic photocycloadditions to date, has approached this problem by designing elegant reactions in which the catalyst-substrate complex absorbs light at longer wavelengths than the free substrate. This has been accomplished either by using a chiral hydrogen-bonding xanthone-based photosensitizer (*13*–*15*) or by using a chiral Lewis acid catalyst capable of inducing a bathochromic shift in the bound substrate (*16*, *17*). In both cases, Bach has achieved impressive enantioselectivities with substoichiometric chiral controllers. However, effective stereocontrol requires careful irradiation with a monochromatic light source that selectively excites the catalyst-substrate complex at a wavelength where absorption by the free substrate is minimized. The contribution of background reaction, though lessened in these systems, nevertheless remains appreciable and results in a dependence of the ee on catalyst concentration; optimal selectivities are obtained only at high catalyst loadings (typically ~50 mol %) at which the catalyzed process can outcompete the racemic background cycloaddition. Thus, the lack of a general strategy for completely eliminating uncatalyzed background photochemistry continues to be a fundamental impediment to the discovery of efficient enantioselective catalytic photocycloadditions.

Given these considerations, we speculated that the visible light–induced (*18*) photocatalytic [2 + 2] cycloaddition (*19*, *20*) recently reported in our laboratory (Fig. 1B) might be an ideal platform for the development of a highly enantioselective catalytic photocycloaddition that is free of racemic background reaction. The crucial activation step in this cycloaddition involves the one-electron reduction of a Lewis acid–activated aryl enone by a Ru(I) complex generated by visible-light irradiation of $Ru(bpy)_3^{2+}$ in the presence of an amine donor. There are two distinct features of this process that together prevent uncatalyzed background reactions. First, $Ru(bpy)_3^{2+}$ is activated by visible light (λ_{max} = 450 nm) at wavelengths where the enone substrates do not absorb (*21*); direct photoexcitation of the enone does not occur with the household white light sources applied in our studies. Second, a Lewis acid ($LiBF_4$) is an essential additive for cycloaddition to proceed; the Li^+ cation presumably activates the enone substrate toward one-electron reduction and stabilizes the resulting radical anion species (*22*). We hypothesized, therefore, that a dual-catalyst system consisting of $Ru(bpy)_3^{2+}$ and an appropriate chiral Lewis acid cocatalyst would promote highly enantioselective [2 + 2] cycloadditions without the complications arising from uncatalyzed background photoreactions.

In our initial screen of Lewis acids, we found that trivalent lanthanide salts such as $Gd(OTf)_3$ were particularly effective cocatalysts for the production of [2 + 2] cycloadducts **2** and **3** (Fig. 1C, entry 1). This observation is consistent with the high kinetic lability of lanthanides (*23*), which may aid catalyst turnover by facilitating displacement of the bidentate product by a monodentate enone substrate. Next, we evaluated a series of Gd complexes bearing chiral ligands that we hoped would influence the stereochemistry of the [2 + 2] cycloaddition. Unfortunately, several ligand classes (e.g., **4**–**6**) that have been effective in previously reported Lewis acid–catalyzed enantioselective transformations (*24*) provided negligible ee's in this reaction (entries 2 to 4). By contrast, Schiff base dipeptide ligand **7**, originally reported by Hoveyda for Cu-catalyzed asymmetric allylic alkylation (*25*), provided [2 + 2] cycloadduct **2** with promising ee (entry 5). To our knowledge, this class of ligand has not previously been used in lanthanide-catalyzed asymmetric reactions; however, its modular structure (*26*) facilitated the rapid synthesis and evaluation of a small library of ligands composed of various salicylaldehyde and amino acid units. A Lewis acid cocatalyst composed of the optimal ligand (**8**) and $Gd(OTf)_3$ afforded cyclobutane **2** in 56% ee (entry 6). Further optimization studies revealed that by replacing the Gd salt with $Eu(OTf)_3$ and by performing the reaction at lower temperatures, the ee of **2** could be increased to 92% (entries 7 to 9).

The optimized conditions require 5 mol % $Ru(bpy)_3Cl_2$ as a visible-light photocatalyst and 10 mol % of a Lewis acid complex composed of a 1:2 ratio of $Eu(OTf)_3$ and chiral ligand **8**. A series of control experiments verify the necessity of each reaction component (Fig. 2A). In the absence of light, photocatalyst, or Lewis acid catalyst, either singularly or in combination, no product is formed and enone substrate **1** can be recovered in good yield. Yet, although the rate of cycloaddition is dependent on the concentration of Lewis acid catalyst, there is no noticeable impact on the ee of the product. Catalyst loadings varying from 2.5 to 20 mol % produced cycloadduct **2** with the same ee in each case (Fig. 2B). These experiments indicate that all of the [2 + 2] cycloadduct is being formed via a pathway involving the chiral Lewis acid and that there is no contribution from a competitive racemic background process, consistent with our design plan.

Previous approaches toward asymmetric catalytic photocycloaddition reactions have exhibited rather limited scope. Minor modifications

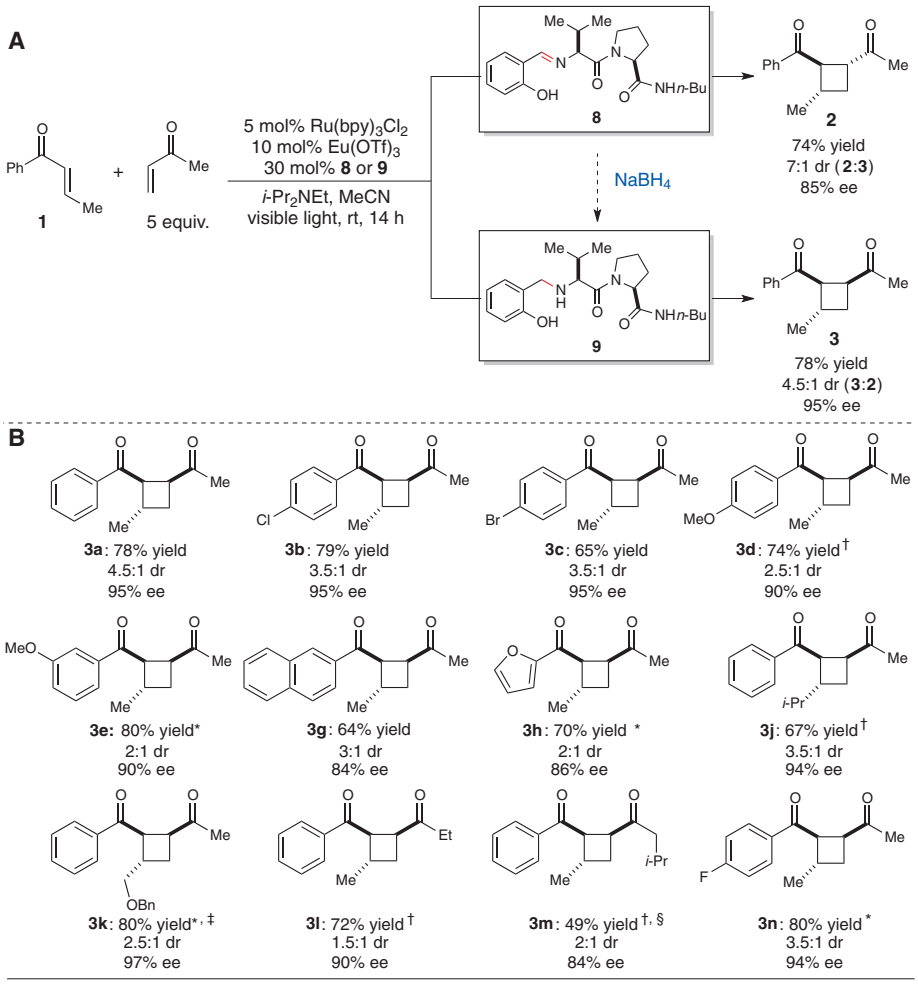

Fig. 4. Diastereocontrol through independent modification of chiral Lewis acid structure. (**A**) Stereoselective access to 1,2-*cis* cycloadducts **3** through reduction of chiral Schiff base ligand **8** to amine **9**. (**B**) Substrate scope of 1,2-*cis* cyclobutanes via enantioselective [2 + 2] photocycloaddition. Diastereomer ratios measured by ^{1}H-NMR analysis of the unpurified reaction mixtures. Reported yields represent total isolated yields of the 1,2-*cis* and 1,2-*trans* isomers. For each entry, yields represent the average of two reproducible experiments. *Reaction conducted for 14 hours. †Reaction conducted for 36 hours. ‡Reaction conducted at 37°C. §Isolated yield of only *cis* isomer.

to the substrate can result in substantial spectral changes that affect the ability to selectively photoexcite the catalyst-bound substrate (*15*). In contrast, the results summarized in Fig. 3 demonstrate that our dual-catalytic system tolerates wide-ranging structural variation (*27*). Successful substrates include aryl enones bearing electron-donating and -withdrawing substituents, heteroaryl enones, and γ-substituted enones. The enantioselectivity remains high for all of these cycloadducts regardless of the ultraviolet (UV) absorptivity of the substrates (*28*). For example, the phenyl and naphthyl enones leading to cyclobutanes **2a** and **2g** both provide high ee even though the UV absorption of the latter extends to considerably longer wavelengths (fig. S1). Consistent with our studies of racemic crossed enone cycloadditions (*20*), we observe the formation of readily separable by-products arising from competitive reductive coupling and aryl enone homodimerization processes. The use of a fivefold excess of the aliphatic enone increases the overall rate of formation of [2 + 2] cycloadducts and minimizes the formation of homocoupling products. Overall, these results represent a substantial improvement in the structural variety of enantioenriched [2 + 2] cycloadducts available by catalysis. Each of the previous reports of asymmetric catalytic photocycloadditions has involved intramolecular reactions of cyclic enone substrates and thus furnished bicyclic products. Our intermolecular cycloaddition of acyclic enones can produce a diverse range of simple monocyclic cyclobutane products in good ee.

One important advantage of this dual-catalytic system is the functional independence of the photocatalyst and the chiral Lewis acid catalyst (*29*). Extensive variations can be made to the structure of the chiral Lewis acid without any deleterious effect on the photochemical properties of the $Ru(bpy)_3^{2+}$ chromophore. This feature facilitates both the optimization of the enantioselectivity and the discovery of complementary reactivity. For example, reduction of Schiff base ligand **8** with $NaBH_4$ afforded secondary amine ligand **9**, the $Eu(OTf)_3$ complex of which was also a highly enantioselective Lewis acid cocatalyst for [2 + 2] cycloaddition. These conditions, however, favored the formation of 1,2-*cis* diastereomer **3** in good ee (Fig. 4A) (*30*). The scope of the cycloaddition using **9** exhibits the same general breadth as reactions conducted with ligand **8** (Fig. 4B), but with complementary diastereoselectivity (*31*).

These studies demonstrate that transition-metal photocatalysts are compatible with a variety of structurally diverse chiral Lewis acid catalysts. The factors governing the success of chiral Lewis acids in asymmetric catalysis have been studied for decades and are now well-understood (*32*). The ability to combine the power and versatility of chiral Lewis acids with the unique reactivity of photocatalytically generated intermediates has the potential to be a valuable platform for the development of a wide range of broadly useful stereocontrolled reactions.

References and Notes

1. E. N. Jacobsen, A. Pfaltz, H. Yamamoto, *Comprehensive Asymmetric Catalysis* (Springer, Berlin, New York, 1999).
2. I. Ojima, *Catalytic Asymmetric Synthesis* (Wiley, Hoboken, NJ, ed. 3, 2010).
3. J. Iriondo-Alberdi, M. F. Greaney, *Eur. J. Org. Chem.* **2007**, 4801–4815 (2007).
4. N. Hoffmann, *Chem. Rev.* **108**, 1052–1103 (2008).
5. H. Rau, *Chem. Rev.* **83**, 535–547 (1983).
6. Y. Inoue, *Chem. Rev.* **92**, 741–770 (1992).
7. J. A. Le Bel, *Bull. Soc. Chim. Fr.* **22**, 337 (1874).
8. W. Kuhn, E. Knopf, *Naturwissenschaften* **18**, 183 (1930).
9. M. Demuth *et al.*, *Angew. Chem. Int. Ed. Engl.* **25**, 1117–1119 (1986).
10. L. M. Tolbert, M. B. Ali, *J. Am. Chem. Soc.* **104**, 1742–1744 (1982).
11. T. Bach, H. Bergmann, K. Harms, *Angew. Chem. Int. Ed.* **39**, 2302–2304 (2000).
12. F. Toda, H. Miyamoto, S. Kikuchi, *J. Chem. Soc. Chem. Commun.*, 621–622 (1995).

13. C. Müller, A. Bauer, T. Bach, *Angew. Chem. Int. Ed.* **48**, 6640–6642 (2009).
14. M. M. Maturi *et al.*, *Chem. Eur. J.* **19**, 7461–7472 (2013).
15. C. Müller *et al.*, *J. Am. Chem. Soc.* **133**, 16689–16697 (2011).
16. H. Guo, E. Herdtweck, T. Bach, *Angew. Chem. Int. Ed.* **49**, 7782–7785 (2010).
17. R. Brimioulle, T. Bach, *Science* **342**, 840–843 (2013).
18. C. K. Prier, D. A. Rankic, D. W. MacMillan, *Chem. Rev.* **113**, 5322–5363 (2013).
19. M. A. Ischay, M. E. Anzovino, J. Du, T. P. Yoon, *J. Am. Chem. Soc.* **130**, 12886–12887 (2008).
20. J. Du, T. P. Yoon, *J. Am. Chem. Soc.* **131**, 14604–14605 (2009).
21. K. Kalyanasundaram, *Coord. Chem. Rev.* **46**, 159–244 (1982).
22. F. Fournier, M. Fournier, *Can. J. Chem.* **64**, 881–890 (1986).
23. K. Mikami, M. Terada, H. Matsuzawa, *Angew. Chem. Int. Ed.* **41**, 3554–3572 (2002).
24. H. C. Aspinall, *Chem. Rev.* **102**, 1807–1850 (2002).
25. M. A. Kacprzynski, A. H. Hoveyda, *J. Am. Chem. Soc.* **126**, 10676–10681 (2004).
26. A. H. Hoveyda, *Chem. Biol.* **5**, R187–R191 (1998).
27. Consistent with our prior studies, crossed [2 + 2] cycloadditions can be achieved with one aryl enone that can easily be reduced to the corresponding radical anion and a second β-unsubstituted alkyl enone that possesses a more negative redox potential but is a less sterically encumbered Michael acceptor.
28. The absolute configuration of **2c** was determined by x-ray crystallographic analysis of the corresponding 2,4-dinitrophenylhydrazone (**S3**) using anomalous dispersion. See supplementary materials for details. The configurations of other 1,2-*trans* cycloadducts were assigned by analogy.
29. A. E. Allen, D. W. MacMillan, *Chem. Sci.* **2012**, 633–658 (2012).
30. Reactions conducted with ligand **9** at –20 °C proceeded at prohibitively slow rates and offered little improvement in ee.
31. The absolute configuration of **3c** was determined by x-ray crystallographic analysis using anomalous dispersion. See supplementary materials for details. The configurations of other 1,2-*cis* cycloadducts were assigned by analogy.
32. H. Yamamoto, *Lewis Acids in Organic Synthesis* (Wiley-VCH, Weinheim, New York, 2000).

Acknowledgments: We thank B. S. Dolinar and I. A. Guzei for determining absolute stereochemistry by x-ray crystallography. Metrical parameters for the structures of **3c** and **S3** are available free of charge from the Cambridge Crystallographic Data Centre under reference numbers CCDC-988977 and 988978, respectively. Funding for this work was provided by an NIH research grant (GM095666) and a postdoctoral fellowship to D.M.S. (GM105149).

Supplementary Materials

www.sciencemag.org/content/344/6182/392/suppl/DC1
Materials and Methods
Supplementary Text
Figs. S1 to S3
Tables S1 to S16
Scheme S1
References (*33*–*43*)

29 January 2014; accepted 10 March 2014
10.1126/science.1251511

Detection of the Gravitational Lens Magnifying a Type Ia Supernova

Robert M. Quimby,[1]* Masamune Oguri,[1,2] Anupreeta More,[1] Surhud More,[1] Takashi J. Moriya,[3,4] Marcus C. Werner,[1,5] Masayuki Tanaka,[6] Gaston Folatelli,[1] Melina C. Bersten,[1] Keiichi Maeda,[7] Ken'ichi Nomoto[1]

Objects of known brightness, like type Ia supernovae (SNIa), can be used to measure distances. If a massive object warps spacetime to form multiple images of a background SNIa, a direct test of cosmic expansion is also possible. However, these lensing events must first be distinguished from other rare phenomena. Recently, a supernova was found to shine much brighter than normal for its distance, which resulted in a debate: Was it a new type of superluminous supernova or a normal SNIa magnified by a hidden gravitational lens? Here, we report that a spectrum obtained after the supernova faded away shows the presence of a foreground galaxy—the first found to strongly magnify a SNIa. We discuss how more lensed SNIa can be found than previously predicted.

A peculiar supernova, PS1-10afx, was discovered by the Panoramic Survey Telescope & Rapid Response System 1 (Pan-STARRS1) on 31 August 2010 (universal time) (*1*). The unusually red color of the object spurred the Pan-STARRS1 team to conduct an array of follow-up observations, including optical and near-infrared spectroscopy, which yielded a redshift of $z = 1.39$. Combined with relatively bright photometric detections, this redshift would imply a peak luminosity of 4×10^{44} erg s^{-1}, which is 400 times brighter than the typical core-collapse supernova. A rare class of superluminous supernovae (SLSN) (*2*) have shown similarly high bolometric outputs, but PS1-10afx distinguishes itself from all other SLSN on two important counts: PS1-10afx is much redder (cooler) and evolved much faster than any SLSN. A generic feature of SLSN models (*3*–*9*) is that they employ high temperatures (T) and/or large photospheric radii (R) to generate high luminosities (L) (recalling that $L \propto T^4R^2$). The observations of PS1-10afx do not fit with these models, suggesting that if it is a SLSN, it is in a class of its own.

An alternate hypothesis (*10*) is that PS1-10afx is actually a regular type Ia supernova (SNIa) with a normal luminosity, but its apparent brightness has been magnified by a gravitational lens. Spectra of PS1-10afx are well fit by normal SNIa templates, as are the colors and light curve shapes. However, normal SNIa exhibit a tight relation between the widths of their light curves and their peak luminosities (*11*–*14*), and PS1-10afx appears 30 times brighter than expected, according to this relation. Such a large magnification of brightness can only occur naturally from strong gravitational lensing, whereby the light emanating from the supernova is bent to form an Einstein-Chwolson ring, or several discrete magnified images (typically two or four) if the alignment is not axisymmetric. Pan-STARRS1 has surveyed sufficient volume to expect such a chance alignment (*15*, *16*), and it is possible that the angular extent of the lensed images was simply too small to be resolved by the observations available. However, for this hypothesis to be confirmed, we must explain why the existing observations give such conclusive photometric and spectroscopic evidence for the presence of the supernova's host galaxy, but the same observations fail to obviously indicate the presence of a foreground lens.

We used the Keck-I telescope with the Low-Resolution Imaging Spectrograph (LRIS) (*17*) with the upgraded red channel (*18*) to observe the host galaxy and any foreground objects at the sky position of PS1-10afx on 7 September 2013 (see fig. S1) (*16*). As illustrated in Fig. 1, there are two narrow emission features that persist at the location of PS1-10afx now that the supernova itself has faded away. The [O II] emission doublet ($\lambda\lambda$ = 3726.1, 3728.8 Å in the rest frame) from the host galaxy previously identified (*1*) is clearly recovered (fig. S2), but we additionally detected a second emission line at ~7890 Å. Because there are no strong emission lines expected from the host at this wavelength (~3300 Å in the host frame), this detection suggests the presence of a second object coincident with PS1-10afx.

The most probable identification for the 7890 Å feature is [O II] at $z = 1.1168 \pm 0.0001$. At this redshift, other strong emission lines such as H-β or [O III] would lie outside of our wavelength coverage. However, as depicted in Fig. 1, we detected a Mg II absorption doublet ($\lambda\lambda$ = 2795.5, 2802.7 Å in the rest frame) at $z = 1.1165 \pm 0.0001$. Blueshifted absorption outflows are typical of star-forming galaxies (*19*), so this estimate is compatible with that derived from the emission lines. We also identify possible Mg I (λ = 2853.0)

[1]Kavli Institute for the Physics and Mathematics of the Universe (WPI), Todai Institutes for Advanced Study, The University of Tokyo, 5-1-5 Kashiwanoha, Kashiwa-shi, Chiba 277-8583, Japan. [2]Department of Physics, The University of Tokyo, Tokyo 113-0033, Japan. [3]Argelander Institute for Astronomy, University of Bonn Auf dem Hügel 71, D-53121 Bonn, Germany. [4]Research Center for the Early Universe, Graduate School of Science University of Tokyo, Hongo 7-3-1, Bunkyo, Tokyo 113-0033, Japan. [5]Department of Mathematics, Duke University, Durham, NC 27708, USA. [6]National Astronomical Observatory of Japan 2-21-1 Osawa, Mitaka, Tokyo 181-8588, Japan. [7]Department of Astronomy, Kyoto University, Kitashirakawa-Oiwake-cho Sakyo-ku, Kyoto 606-8502, Japan.

*Corresponding author. E-mail: robert.quimby@ipmu.jp